frontiers in Materials

ORIGINAL RESEARCH
published: 27 November 2020
doi: 10.3389/fmats.2020.588716

The Influence of Si_3N_{4w} Volume Fraction on the Microstructure and Properties of Si_3N_{4w}/Si_3N_4 Composites via CVI Technique

Chao Chen[1], *Yongsheng Liu*[1,2]*, *Wei Yue*[1], *Fang Ye*[1], *Jing Wang*[1] *and Qingfeng Zeng*[1]

[1]Science and Technology on Thermostructural Composite Materials Laboratory, Northwestern Polytechnical University, Xi'an, China, [2]NPU-SAS Joint Research Center of Advanced Ceramics, Northwestern Polytechnical University, Xi'an, China

Wave-transparent ceramic composites with excellent comprehensive performances are of particular significance for the development of space vehicles. In this study, Si_3N_{4w} was prepared by the gel-casting process and then combined with chemical vapor infiltration (CVI)-obtained Si_3N_4 to yield Si_3N_{4w}/Si_3N_4 composites with five Si_3N_{4w} volume fractions. The influence of the Si_3N_{4w} volume fraction on the microstructures, mechanical properties, and dielectric characteristics of the Si_3N_{4w}/Si_3N_4 composites were all studied. The results showed that Si_3N_{4w}/Si_3N_4 composites possess A sandwich structures. Higher Si_3N_{4w} volume fractions led to less incorporated amounts of the Si_3N_4 matrix at the same depth. The 25 vol% Si_3N_{4w}/Si_3N_4 composites integrated relatively higher Si_3N_{4w} volume fraction and load transfer ability of the matrix, leading to better flexural strengths reaching up to 41.37 MPa. The dielectric constants of the five prepared Si_3N_{4w}/Si_3N_4 composites ranged from 2.25 to 4.0. The dielectric losses were all lower than 0.005, demonstrating the good dielectric properties of the Si_3N_{4w}/Si_3N_4 composites.

Keywords: Si_3N_{4w}/Si_3N_4 composites, gel-casting, chemical vapor infiltration, dielectric properties, mechanical properties

OPEN ACCESS

Edited by:
Yang Bai,
University of Oulu, Finland

Reviewed by:
Yan Zhang,
Central South University, China
Subhasis Roy,
University of Calcutta, India

***Correspondence:**
Yongsheng Liu
yongshengliu@nwpu.edu.cn

Specialty section:
This article was submitted to Ceramics and Glass, a section of the journal Frontiers in Materials

Received: *29 July 2020*
Accepted: *19 October 2020*
Published: *27 November 2020*

Citation:
Chen C, Liu Y, Yue W, Ye F, Wang J and Zeng Q (2020) The Influence of Si_3N_{4w} Volume Fraction on the Microstructure and Properties of Si_3N_{4w}/Si_3N_4 Composites via CVI Technique. Front. Mater. 7:588716. doi: 10.3389/fmats.2020.588716

INTRODUCTION

High-temperature wave-transparent materials are used in spacecraft radomes and antenna windows, which require good mechanical and dielectric properties, as well as high-temperature resistance. Therefore, the development of novel wave-transparent materials with elevated wave transmittance and strength is of great significance for advanced and reliable applications (Medding, 1996; Bolivar et al., 2003; Ashok et al., 2007; Kandi et al., 2014; Hehdari et al., 2017).

Si_3N_4-based ceramics are employed in wave-transparent materials due to their excellent comprehensive performances (Arakawa et al., 1991; Hsieh and Mizuhara, 1987; Hsieh, 1987; Zou et al., 2009). For instance, Xu et al. (2020) studied the influence of different sintering additives on the dielectric properties of reaction-bonded Si_3N_4. Their results showed that the addition of Y_2O_3 and La_2O_3 powders may generate Y-Si-O-N and La-Si-O-N phases, further increasing the dielectric constant and dielectric loss Lee et al. (2000) prepared a Si_3N_4w/Si_3N_4 composite by the Gas Pressure Sintering (GPS) method. The amount of β-Si_3N_4w changed the microstructure, which changed the thermal conductivity. Ding et al. (2007) sintered Si_3N_4 powders at 1,200–1,500°C under air to yield prepared Si_3N_4 ceramics with a SiO_2 coating on the surface. The influence of sintering temperature and holding time on the oxidation degree, porosity, flexural

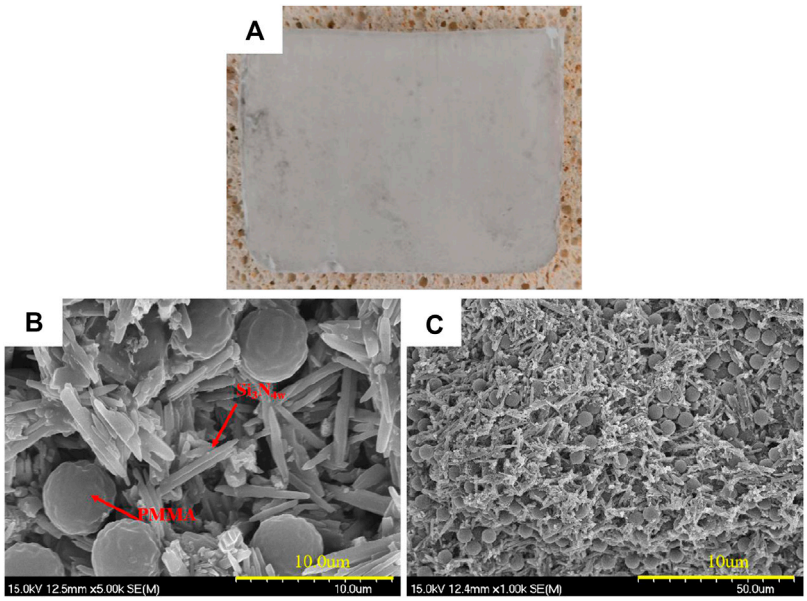

FIGURE 1 | Morphology of the Si_3N_{4w} preform before decarbonization: **(A)** macro photo; **(B)** high magnification SEM photo of section; **(C)** low magnification SEM photo of section.

strength, and dielectric properties were all studied. The highest flexural strength of prepared Si_3N_4 ceramics reached 136.9 MPa and the lowest dielectric constant was 3.1.

To synergistically improve the mechanical and dielectric properties, the development of silicon nitride-based wave-transparent composite materials is increasingly considered (Cao et al., 2013; Wan et al., 2016). For example, Yang et al. (2019) (Li et al., 2019) prepared unidirectional silicon nitride fiber-reinforced silica composites by monofilament winding combined with the sol-gel method. The composite prepared by sintering under an N_2 atmosphere showed the highest flexural strengths reaching up 210 MPa at 1,200°C. Besides, the flexural strength improved from 160 to 210 MPa at 900°C due to the release of stress in the fiber. Meanwhile, a $Si_3N_{4f}/SiON/SiO_2$ composite has been prepared by introducing a SiON interphase using the precursor transformation method. After decarbonization by annealing, the flexural strength of $Si_3N_{4f}/SiON/SiO_2$ decreased by 35% when compared to Si_3N_{4f}/SiO_2 but the fracture toughness improved. Cheng et al. (2019) assembled porous Si_3N_4/Si_3N_4 composites by 3D printing combined with the chemical vapor infiltration (CVI) method. The increase in CVI processing to 12 h led to a decline in the porosity from 68.65 to 12.07. Meanwhile, the dielectric constant increased from 1.72 to 3.6 but the dielectric loss was always lower than 0.01. Since 2003, polysilazane has been used as a precursor in combination with the polymer infiltration pyrolysis process to prepare SiO_{2f}/Si_3N_4 with good mechanical and high-temperature dielectric properties (Qi et al., 2005a; Qi et al., 2005b; Qi et al., 2005c).

However, extremely high or low volume fractions of reinforcement in the ceramic matrix composites should lead to the declined mechanical properties of the resulting composite materials. Besides, different reinforcement volume fractions should result in variable contents and distributions of reinforcement, as well as various matrices and pores, further influencing the dielectric properties of the composites. Therefore, clarifying the influencing rules of the reinforcement volume fractions on the mechanical and dielectric properties of ceramic matrix composites is highly desirable for advanced applications.

Li et al. (2020) prepared zirconia fiber hybrid alumina fiber/boron phenolic (ZA/BPF) composites with fiber volume fractions of 5, 10, 15, 25, and 30 vol%. The microscopic results showed that extremely low and high reinforcement volume fractions resulted in weak bonding between the matrix and fiber. At a fiber volume fraction of 25%, the maximum flexural strengths of the composites reached 48.86 MPa. Using the hot-pressing sintering method, Xu et al. (1994) prepared SiC_f/Si_3N_4 with a fiber volume fraction of 14, 29, and 55 vol%. Their data suggested that the flexural strength of the composites first increased with the fiber volume fraction and then decreased. The reason for the reduction in strength was related to the fiber damage caused by its contact during the hot-pressing process of high volume fraction composites.

In this work, five preforms of Si_3N_{4w} volume fractions (5, 15, 25, 35, and 45 vol%) were prepared by the gel-casting process. Different volume fractions of the Si_3N_{4w}/Si_3N_4 composites were then obtained by introducing a Si_3N_4 matrix through the CVI Si_3N_4 process. The effects of whisker volume fractions on the microstructures, mechanical properties, and dielectric characteristics of the Si_3N_{4w}/Si_3N_4 composites were all studied. The results suggested that the 25 vol% Si_3N_{4w}/Si_3N_4 possessed the highest comprehensive performances.

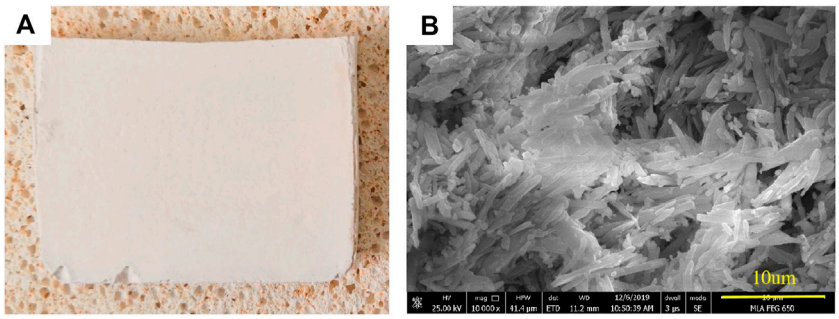

FIGURE 2 | Morphology of Si_3N_{4w} after decarbonization: **(A)** macro photo; **(B)** SEM photo.

EXPERIMENT

Raw Materials

Water-based gel casting was used to prepare the Si_3N_{4w} preforms with different volume fractions. Firstly, Si_3N_4w was used to configure the Si_3N_4w slurry, then PMMA was added after ball milling for 4 h. Subsequently, the slurry was heated at 70°C to cure for 2 h. After drying, it was discharged at 400°C to create the Si_3N_4w performs. Si_3N_{4w} with a length of 4–12 μm (average 8 μm), diameter of 0.8–1.2 μm (average 1 μm), and average aspect ratio of 8:1 was prepared in our laboratory. Polymethyl methacrylate (PMMA; Wuhan Yuancheng Technology Development Co., Ltd.) was employed as the pore former, acrylamide (Tianjin Comeo Chemical Reagent Co., Ltd.) as a monomer, and methylenebisacrylamide (MACLIN) as a crosslinking agent.

$SiCl_4$-NH_3-H_2-Ar was utilized as a gas source system for the preparation of the Si_3N_4 matrix by CVI, $SiCl_4$ as a source of Si element, and H_2 as a carrier and dilution gas. In this process, H_2 was passed through the liquid $SiCl_4$ to take the saturated $SiCl_4$ vapor into the reaction furnace in actual production. NH_3 was employed as a source of N element and Ar as a dilution gas. $SiCl_4$, H_2, and Ar with a purity of 99.999 vol% were all obtained from the Sichuan Messer Gas Products Co., Ltd., Xi'an branch. NH_3 (purity 99.99 vol%) was purchased from the Beijing Marty Technology Co., Ltd.

Experimental Process

Sizing agents with Si_3N_{4w} volume fractions of 5, 15, 25, 35, and 45 vol% were prepared to yield preforms with Si_3N_{4w} volume fractions of 10, 20, 30, 40, and 50 vol% after solidification and decarbonization processes, respectively. To prevent over-shrinkage during the preparation of preforms at low volume fractions of Si_3N_{4w}, PMMA was added as a pore former in the sizing agent.

Using the CVI Si_3N_4 process, Si_3N_{4w}/Si_3N_4 composites with five-volume fractions of Si_3N_{4w} preforms were prepared and placed in the graphite mold. The CVI process are described in detail in literature (Zhou et al., 2019a). The preparation process was divided into six periods, each consisting of 60 h. For the convenience of subsequent expressions, the abbreviation 15 vol% Si_3N_{4w}/Si_3N_4 represented the composite prepared using the size agent with 15 vol% Si_3N_{4w}, the same as the other composites. The influences of volume fractions of Si_3N_{4w} on the microstructures, mechanical properties, and dielectric characteristics of Si_3N_{4w}/Si_3N_4 were all studied.

Characterization

The density and porosity of each sample were tested by the Archimedes drainage method using AG204 electronic analytic balance by Mettler Toledo (accuracy 0.0001 g). The microstructures were viewed by a Helios G4 CX focused ion-electron double beam electron microscope (FEI). The flexural strength and fracture toughness values at loading speeds of 0.5 and 0.05 mm/min were obtained by the SANS CMT4304 electronic universal testing machine. The dielectric properties were tested by a vector network analyzer (MS4644A, produced by Anritsu, Japan). The experiments were performed at a standard dielectric sample size of 22.86 mm × 10.16 mm × *h* mm and a testing frequency band of 8.2–12.4 GHz.

RESULTS AND DISCUSSION

Microstructure

The morphology of the Si_3N_{4w} preform before decarbonization is shown in **Figure 1**. The macro photo of the Si_3N_{4w} preform before decarbonization displayed a polymer matrix composite of certain strength and hardness, and it can be transferred without being destroyed after forming (**Figures 1A**). The smooth and flat surface revealed the advantages of the gel-casting in terms of near net-size forming. The high magnification SEM photo in **Figures 1B** exhibits the intact structures of Si_3N_{4w} and PMMA. The PMMA sphere with a diameter of approximately 5 μm could support the whisker structure. The low magnification SEM photo in **Figures 1C** reveals evenly dispersed dSi_3N_{4w} and PMMA, beneficial to the formation of connected pores after decarbonization.

The morphology of the Si_3N_{4w} preform after decarbonization is shown in **Figure 2**. The preform kept a perfectly consistent appearance during the decarbonization process (**Figures 2A**). In the SEM photo of **Figures 2B**, the shape of Si_3N_{4w} was completely preserved and the PMMA spheres were fully decomposed.

TABLE 1 | Si_3N_{4w} volume fraction, bulk density, and open porosity of the five kinds of Si_3N_{4w} preform after decarbonization.

Si_3N_{4w} volume fraction in size agent (vol%)	Si_3N_{4w} volume fraction in preform after decarbonization (vol%)	Bulk density (g/cm^3)	Open porosity (vol%)	Close porosity (vol%)
5	13.0	0.42	86.5	0.5
15	19.9	0.64	79.7	0.4
25	29.2	0.93	69.5	1.3
35	38.5	1.23	60.3	1.2
45	46.8	1.50	52.7	0.5

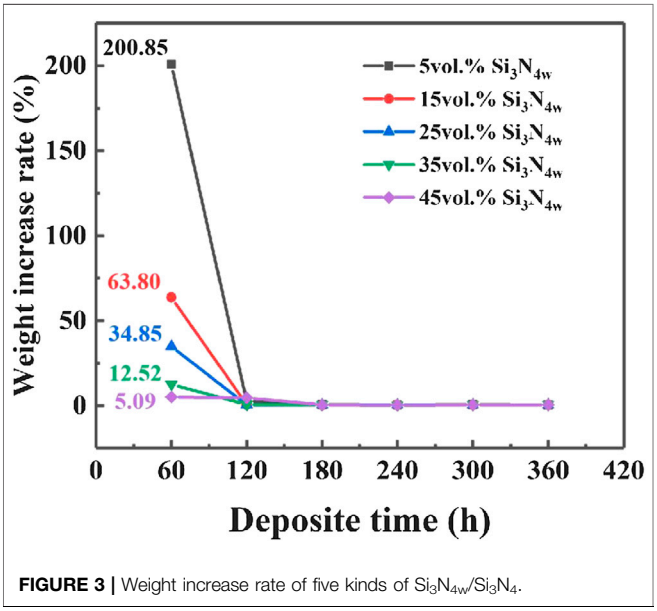

FIGURE 3 | Weight increase rate of five kinds of Si_3N_{4w}/Si_3N_4.

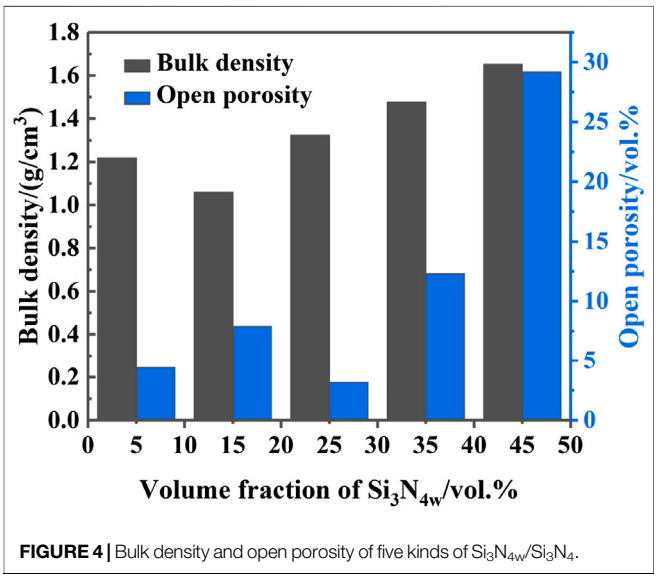

FIGURE 4 | Bulk density and open porosity of five kinds of Si_3N_{4w}/Si_3N_4.

The Si_3N_{4w} volume fractions, bulk densities, and open porosities of the five prepared Si_3N_{4w} preforms after decarbonization are listed in **Table 1**. The Si_3N_{4w} volume fractions of the five preforms all increased due to the inevitable shrinkage during the solidification and decarbonization processes. Lower Si_3N_{4w} volume fractions in the sizing agent led to larger increasing rates of Si_3N_{4w} volume fractions in the preforms after decarbonization. In turn, the increase in the actual Si_3N_{4w} volume fraction in the preform led to a rise in bulk density from 0.42 to 1.50 g/cm^3. By comparison, the open porosity declined from 86.5 to 52.7 vol %. The close porosity of the five preforms were all approximately 1 vol%, confirming the high connectivity of pores inside the preforms.

The weight increasing rates of five Si_3N_{4w}/Si_3N_4 composites are presented in **Figure 3**. All Si_3N_4 matrices were almost incremented in the first furnace deposition. Thus, the diffusion channels of deposition gas in the preforms became closed after the process. The subsequent deposition process ensured complete densification of all five Si_3N_{4w}/Si_3N_4 under the deposition conditions. Lower Si_3N_{4w} volume fractions led to larger weight increasing rates of Si_3N_{4w}/Si_3N_4, as well as significant differences between different Si_3N_{4w}/Si_3N_4. The weight increasing rate of 5 vol% Si_3N_{4w}/Si_3N_4 in the first furnace deposition reached 200.85%, while that of 45 vol% Si_3N_{4w}/Si_3N_4 was only 5.09%. The reason for this had to do with the light weight and large porosity of the low Si_3N_{4w} volume fraction composite.

The bulk densities and open porosities of five prepared Si_3N_{4w}/Si_3N_4 composites are depicted in **Figure 4**. The bulk density of 5 vol% Si_3N_{4w}/Si_3N_4 was larger than that of 15 vol% Si_3N_{4w}/Si_3N_4. For other samples, larger Si_3N_{4w} volume fractions induced elevated bulk densities. The highest bulk density was recorded with 45 vol% Si_3N_{4w}/Si_3N_4 (1.65 g/cm^3), while the lowest was obtained with 15 vol% Si_3N_{4w}/Si_3N_4 (1.06 g/cm^3). The general rule of open porosity stated that higher Si_3N_{4w} volume fractions should yield larger open porosities. However, the high open porosity of 45 vol% Si_3N_{4w}/Si_3N_4 appeared to contradict the low porosity and small pore size of the 45 vol% Si_3N_{4w} preform.

To explain the above abnormal phenomenon, the surface morphologies of 45 and 25 vol% Si_3N_{4w}/Si_3N_4 were studied and the results are gathered in **Figure 5**. Numerous cracks were distributed on the surface of 45 vol% Si_3N_{4w}/Si_3N_4 (**Figures 5B**). The widths of the cracks were around 100 nm (**Figures 5B**). However, no cracks were noticed on the surface of 25 vol% Si_3N_{4w}/Si_3N_4 (**Figures 5C, D**). Therefore, the surface cracks caused the elevated open porosity of 45 vol% Si_3N_{4w}/Si_3N_4. The difference between

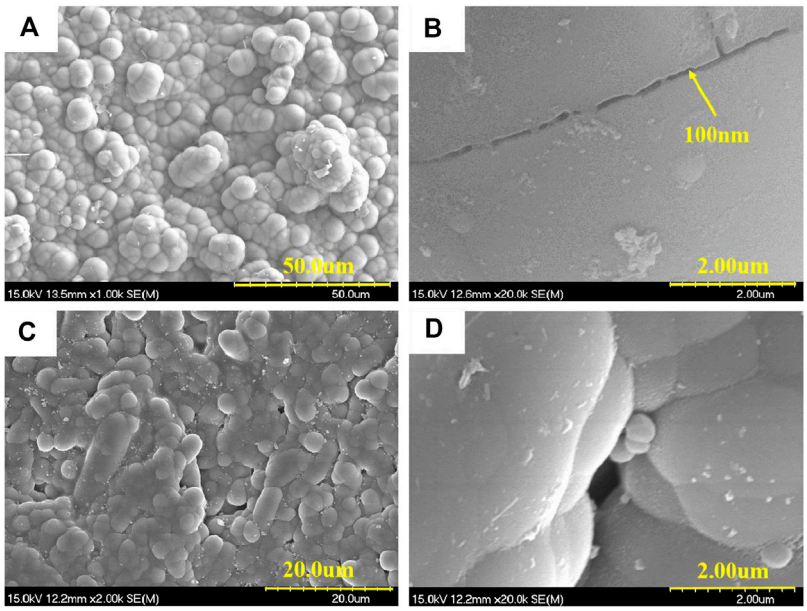

FIGURE 5 | Surface morphology of 45 and 25 vol% Si_3N_{4w}/Si_3N_4: **(A)** surface crack distribution of 45 vol% Si_3N_{4w}/Si_3N_4; **(B)** surface crack width of 45 vol% Si_3N_{4w}/Si_3N_4; **(C)** surface crack distribution of 25 vol% Si_3N_{4w}/Si_3N_4; **(D)** surface morphology of 25 vol% Si_3N_{4w}/Si_3N_4.

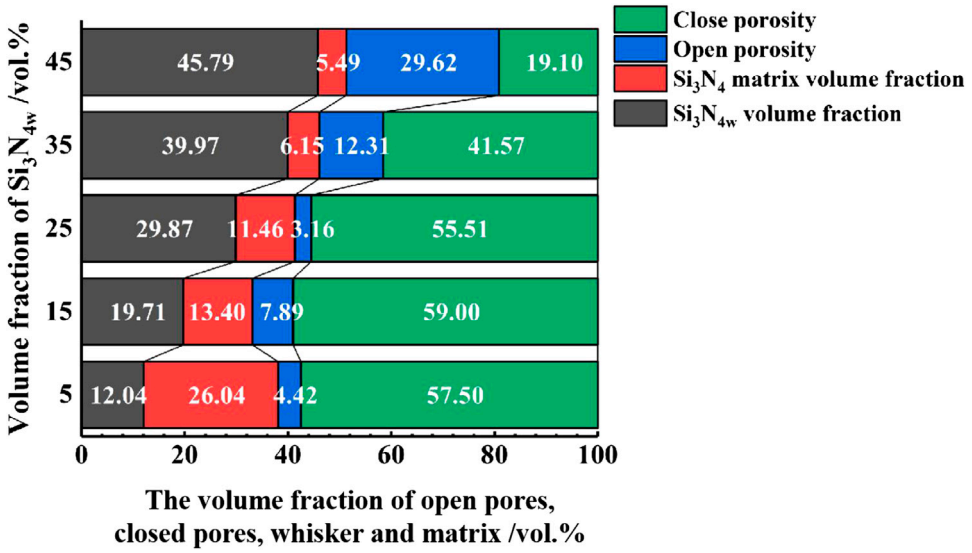

FIGURE 6 | The volume fraction of open pores, closed pores, whisker, and matrix/vol%.

the crystalline Si_3N_{4w} and amorphous CVI Si_3N_4 matrix (Zhou et al., 2019b) should induce differences between the thermal expansion coefficients of Si_3N_{4w} and the Si_3N_4 matrix. Elevated Si_3N_{4w} volume fractions yielded larger differences. Thus, high Si_3N_{4w} volume fraction composites were more prone to surface cracking. The existence of surface cracking would inevitably cause stress concentration and high open porosity, which would decline the ability of rain erosion resistance. On the other hand, the thermal expansion coefficient mismatch brought by the change in the Si_3N_{4w} volume fraction should be taken into consideration during the preparation of wave-transparent composites.

Assuming the density of both Si_3N_{4w} and the Si_3N_4 matrix as 3.2 g/cm^3, the volume fraction of whisker, matrix, open pore, and close pore of the five prepared Si_3N_{4w}/Si_3N_4 composites through weight, bulk density, and open porosity were all obtained. In

Figure 6, the volume fractions of the solid phase of Si_3N_{4w} and the matrix were proportional to bulk densities in **Figure 4**. Lower Si_3N_{4w} volume fractions led to elevated relative contents of the matrix. In turn, higher relative contents of the matrix represented superior load transfer capacities.

Typical macromorphologies of the Si_3N_{4w}/Si_3N_4 samples are displayed in **Figure 7**. The surface of 25 vol% Si_3N_{4w}/Si_3N_4 looked evenly white with a hard texture (**Figures 7A**). The thickness of 25 vol% Si_3N_{4w}/Si_3N_4 was estimated to be approximately 2 mm (**Figures 7B**). Also, two dividing centrosymmetric lines were noticed and both estimated to 0.5 mm from the surface. This confirmed the limited penetration depth of the Si_3N_4 matrix in a specific gel-casting Si_3N_{4w} preform under the CVI Si_3N_4 process.

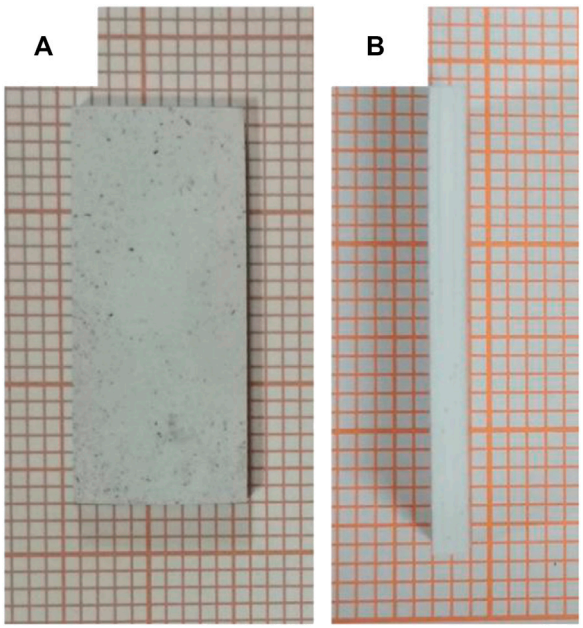

FIGURE 7 | Typical macromorphology of Si_3N_{4w}/Si_3N_4: **(A)** surface of the 25 vol% Si_3N_{4w}/Si_3N_4; **(B)** section of the 25 vol% Si_3N_{4w}/Si_3N_4.

Based on the penetration morphology of **Figures 7B**, the structure of Si_3N_{4w}/Si_3N_4 was simplified as a sandwich construction. The inherent characteristics of the CVI process caused a gradual decline in the content from the surface to the dividing line. The medium part was mainly composed of Si_3N_{4w} with almost no deposited matrix. This structure was similar to the A sandwich structure of a multi-layered radome structure consisting of a high-density side layer and low-density center layer. Materials with sandwich structures often possess high specific strengths and broadband wave-transparent abilities. Meanwhile, the gradient structure of the side layers relieved the stress, which may improve the mechanical properties of the materials. In other words, the whisker preform combined with the CVI process could yield materials with A sandwich and gradient structures.

The section penetration morphologies of the five prepared Si_3N_{4w}/Si_3N_4 ceramics are depicted in **Figure 8**. Four positions (surface, 100, 500, and 1,000 μm distance from the surface) were observed for each sample, and the yellow numbers represent the thickness of the matrix around Si_3N_{4w}. The surfaces of the five prepared Si_3N_{4w}/Si_3N_4 were all covered by dense CVI Si_3N_4. Each Si_3N_{4w}/Si_3N_4 sample revealed that closure of the surface led to less matrix content around Si_3N_{4w}. When the surface is closed, gas cannot enter the preform through the pores, resulting in a reduction of the internal matrix phase. At the same depth, larger Si_3N_{4w} volume fractions induced less matrix content around Si_3N_{4w}. For example, matrix deposition is rarely observed at 35 and 45 vol%. With the increase of the whisker volume fraction, the amount of matrix decreases and the density changes. And the porosity increases gradually. More matrix was

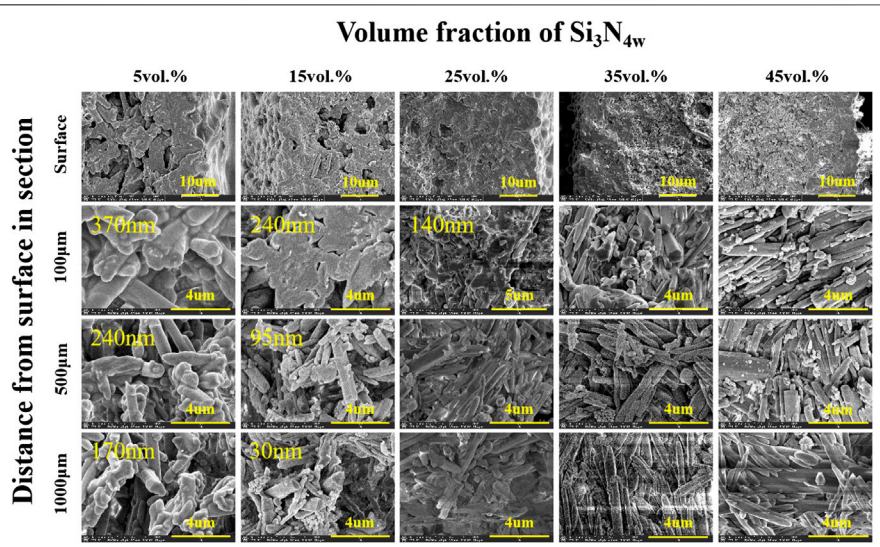

FIGURE 8 | Section penetration morphology of five kinds of Si_3N_{4w}/Si_3N_4.

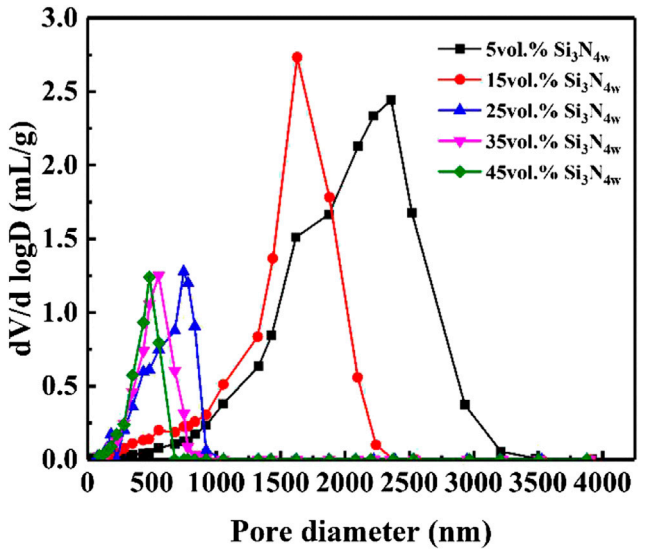

FIGURE 9 | Pore size distribution of Si_3N_{4w}/Si_3N_4.

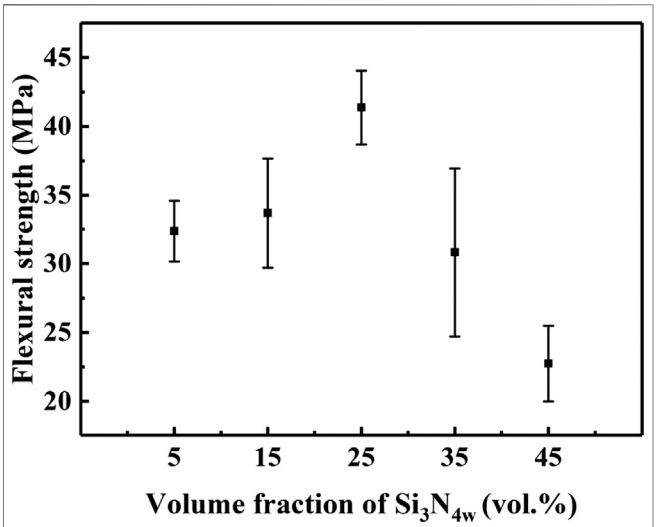

FIGURE 10 | Flexural strength of the five kinds of Si_3N_{4w}/Si_3N_4.

still deposited at 1 mm distance from the surface in 5 and 15 vol% Si_3N_{4w}/Si_3N_4 samples. Likewise, the density and porosity decreased, but this is exactly what is needed to form the sandwich structure mentioned later. By comparison, almost no matrix surrounded Si_3N_{4w} at only 100 μm distance from the surface in 15 vol% Si_3N_{4w}/Si_3N_4.

The pore size distributions of Si_3N_{4w}/Si_3N_4 are gathered in **Figure 9**. The pore sizes of all five Si_3N_{4w}/Si_3N_4 specimens looked normally distributed. As Si_3N_{4w} volume fraction decreased, the pore size became more concentrated at 500, 600, 800, 1,600, and 2,500 nm, respectively. Moreover, lower Si_3N_{4w} volume fractions induced wider pore size distribution ranges. Therefore, the A sandwich structure of Si_3N_{4w}/Si_3N_4 showed that the CVI Si_3N_4 process could not effectively penetrate pores smaller than 2.5 μm in a gel-casting Si_3N_{4w} preform.

Mechanical Properties

The flexural strengths of the five Si_3N_{4w}/Si_3N_4 composites were tested and the results are shown in **Figure 10**. As the Si_3N_{4w} volume fraction increased, the flexural strength of Si_3N_{4w}/Si_3N_4 first rose and then decreased. A maximum strength of 41.37 MPa was recorded with 25 vol% Si_3N_{4w}/Si_3N_4. The minimum flexural strength of 22.74 MPa was registered with 45 vol% Si_3N_{4w}/Si_3N_4. The flexural strengths of different Si_3N_{4w}/Si_3N_4 composites were analyzed by combining the component volume fractions shown in **Figure 6** and section penetration morphologies in **Figure 8**. The 5 and 15 vol% Si_3N_{4w}/Si_3N_4 composites showed higher load transfer abilities due to elevated matrix contents. Therefore, apparent fractures of Si_3N_{4w} can still be seen at 1 mm from the surface. However, the low Si_3N_{4w} volume fractions of 5 and 15 vol% Si_3N_{4w}/Si_3N_4 led to relatively lower flexural strengths. For 35 and 45 vol% Si_3N_{4w}/Si_3N_4, although they possessed elevated Si_3N_{4w} volume fractions, their low load transfer abilities caused by low matrix content significantly decreased their flexural strengths. Furthermore, the flexural strengths of 35 and 45 vol% Si_3N_{4w}/Si_3N_4 were a little lower than those of 5 and 15 vol% Si_3N_{4w}/Si_3N_4, confirming the significant influence of the load transfer ability of the matrix on flexural strength. By contrast, the 25 vol % Si_3N_{4w}/Si_3N_4 ceramic integrated a moderate whisker volume fraction and matrix content, thereby inducing a better strengthening effect and load transfer ability. When the

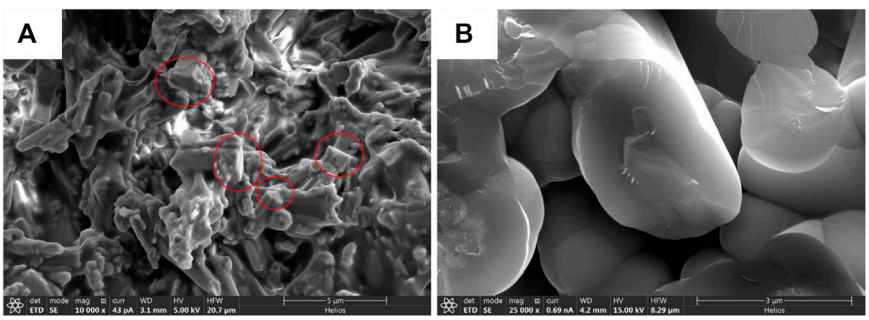

FIGURE 11 | Typical fracture morphology of Si_3N_{4w}/Si_3N_4: **(A)** low magnification SEM photo; **(B)** high magnification SEM photo.

volume fraction of the matrix is too low, the matrix cannot effectively bond and disperse the load, which leads to a decrease of strength. Similarly, when the volume fraction of the whisker is too low, the ability to hinder cracks and other defects is very small and cannot play an enhancement role, resulting in the reduction of strength. However, the volume fraction of 25 vol% is in an intermediate state, which ensures the action of both the matrix and the reinforcer. This, in turn, led to the highest flexural strength.

A typical fracture morphology of Si_3N_{4w}/Si_3N_4 is presented in **Figure 11**. Numerous flat sections can be seen in the low magnification SEM photo. The high magnification photo showed a smooth interface between Si_3N_{4w} and the Si_3N_4 matrix. Obviously, the fracture of Si_3N_{4w}/Si_3N_4 looked typically brittle, inferring the high bonding strength between Si_3N_{4w} and the Si_3N_4 matrix.

The fracture toughness values of the five Si_3N_{4w}/Si_3N_4 samples were tested by a single-notched beam method and the data are gathered in **Figure 12**. The high porosity and hollow sandwich structure of the composites led to very low fracture toughness values. As the Si_3N_{4w} volume fraction increased, the fracture toughness first fell and then rose. The highest value reached only 0.44 MPa $m^{1/2}$ and was recorded with 45 vol% Si_3N_{4w}/Si_3N_4. By comparing the tendency with the component volume fraction in **Figure 6**, the fracture toughness was shown to positively correlate with the total solid content of Si_3N_{4w} and the Si_3N_4 matrix. From another perspective, the fracture toughness negatively correlated with porosity due to the very large bonding strength of the interface of Si_3N_{4w} and the Si_3N_4 matrix, which prevented cracks from deflection. As a result, larger porosity led to lower fraction toughness.

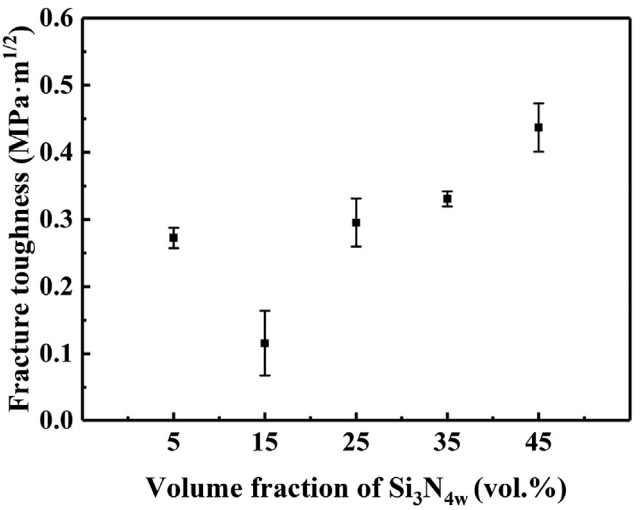

FIGURE 12 | Fracture toughness of the five kinds of Si_3N_{4w}/Si_3N_4.

Dielectric Properties

The room-temperature dielectric properties of the five Si_3N_{4w}/Si_3N_4 specimens are shown in **Figure 13**. The dielectric constant ranged between 2.25 and 4.0, and was positively correlated with the total solid content in **Figure 8**. Therefore, the relative content of the whisker and matrix did not influence the dielectric constant very much. As the whisker volume increases, the real part of the complex dielectric constant increases. From the perspective of the microstructure, with the whisker volume increasing, the pore radius decreases, and the electromagnetic wave scattering in the pore increases. So the dielectric constant increases as the dielectric loss also increases. Also, the dielectric constant values of the Si_3N_4 matrix and Si_3N_{4w} were similar. The dielectric constant lines were approximately straight, showing a slight influence of frequency in the x-band on the dielectric constant.

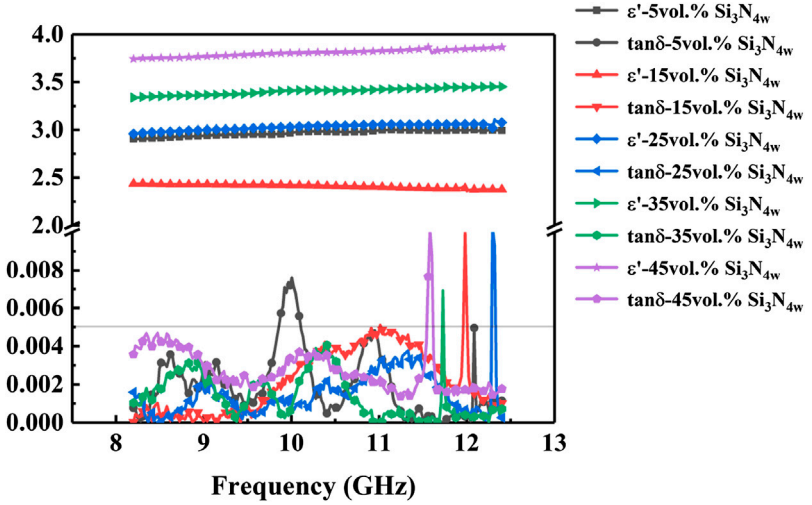

FIGURE 13 | Dielectric properties of the five kinds of Si_3N_{4w}/Si_3N_4.

Limited by the accuracy of the vector network analyzer during testing low-loss materials, the dielectric loss of the five Si_3N_{4w}/Si_3N_4 did not follow obvious rules. However, the dielectric loss of all five composites was less than 0.005, confirming excellent dielectric properties. Besides, the influences of the interface between the Si_3N_4 matrix and Si_3N_{4w} on dielectric loss were slight.

CONCLUSION

The effects of the Si_3N_{4w} volume fraction on the microstructures, mechanical properties, and dielectric characteristics of Si_3N_{4w}/Si_3N_4 were all studies in this paper and the following conclusions could be drawn:

(1) The connectivity of pores in the Si_3N_{4w} preform prepared by the gel-casting process was good due to the small pore size which yielded Si_3N_{4w}/Si_3N_4 with an A sandwich structure. The relative matrix content of 5 vol% Si_3N_{4w}/Si_3N_4 was higher than that of 15 vol% Si_3N_{4w}/Si_3N_4. Higher Si_3N_{4w} volume fractions led to lower relative contents of the Si_3N_4 matrix and less matrix distribution at the same depth. In the sample of the volume fraction of 25 vol%, the content of the matrix and whisker was moderate, and the porosity was the lowest, which made it form an ideal sandwich structure.

(2) Since 25 vol% Si_3N_{4w}/Si_3N_4 integrated a relatively higher Si_3N_{4w} volume fraction and load transfer ability of the matrix, the resulting flexural strength reached the highest value of 41.37 MPa. At a distance of 100 μm from the surface, the matrix thickness around the whisker could still reach 140 nm. The high open porosity led to the low fraction toughness of Si_3N_{4w}/Si_3N_4. The obvious brittle fracture showed a very high interface bonding strength. Therefore, the fracture toughness of Si_3N_{4w}/Si_3N_4 was positively related to the total solid content. The surface of the sample with a 45 vol% whisker also reflected a high density, and the bulk density tended to be the highest. As a result, the fracture toughness of 45 vol% Si_3N_{4w}/Si_3N_4 was the highest (0.44 MPa $m^{1/2}$).

(3) The dielectric constants of Si_3N_{4w}/Si_3N_4 ranged between 2.25 and 4.0, and was positively related to the total solid content. This may infer similar dielectric constants of Si_3N_{4w} and the Si_3N_4 matrix. Dielectric losses were all less than 0.005, showing good dielectric properties of the composites. Besides, the dielectric loss of the interface between Si_3N_{4w} and the Si_3N_4 matrix was slight.

DATA AVAILABILITY STATEMENT

The original contributions presented in the study are included in the article/supplementary material, further inquiries can be directed to the corresponding author.

AUTHOR CONTRIBUTIONS

CC, YL, and WY carried out the concepts, design, definition of intelectual content, literature search data acquisition, data analysis and manuscript preparation. FY, JW, and QZ provided assistance for data accuisition, data analysis and statistical analysis. CC carried out literature search data acquisition and manuscript editing. YL and WY performed manuscript review. All authors have read and approved the content of the manuscript.

FUNDING

This work was supported by the National Key Research and Development Program of China (No. 2018YFB1106600), the Chinese National Foundation for Natural Sciences under Contracts (No.51672217, No.51572224), and the Fundamental Research Funds for the Central Universities (No. 3102019ghxm014).

REFERENCES

Arakawa, T., Mori, T., and Matsumoto, Y. (1991). *Silicon nitride sintered body and process for preparation thereof.* US Patent No 5017530

Ashok, K., Sharma, S., and Ghanshyam, S. (2007). Measurement of dielectric constant and loss factor of the dielectric material at microwave frequencies. *Prog. Electromagn. Res. C* 69, 47–54. doi:10.2528/PIER06111204

Bolivar, P. H., Brucherseifer, M., and Rivas, J. G. (2003). Measurement of the dielectric constant and loss tangent of high dielectric-constant materials at terahertz frequencies. *IEEE Trans. Microw. Theory Tech.* 51 (4), 1062–1066. doi:10.1109/tmtt.2003.809693.

Cao, F., Fang, Z. Y., and Zhang, C. R. (2013). High-temperature properties and associated structure evolution of continuous SiNO fiber-reinforced BN composites for wave transparency. *Mater. Design.* 43, 258–263. doi:10.1016/j.matdes.2012.07.037.

Cheng, Z. L., Ye, F., Liu, Y., Qiao, T., Li, J., Qin, H., et al. (2019). Mechanical and dielectric properties of porous and wave-transparent Si_3N_4-Si_3N_4 composite ceramics fabricated by 3D printing combined with chemical vapor infiltration. *J. Adv. Ceram.* 8 (3), 399–407. doi:10.1007/s40145-019-0322-8.

Ding, S., Zeng, Y., and Jiang, D. (2007). Oxidation bonding of porous silicon nitride ceramics with high strength and low dielectric constant. *Mater. Lett.* 61 (11-12), 2277–2280. doi:10.1016/j.matlet.2006.08.067.

Hehdari, M. S., Ghezavati, J., Abbasgholipour, M., and Mohammadi Alasti, B. (2017). Various types of ceramics used in radome: a review. *Sci. Iran. B* 24 (3), 1136–1147. doi:10.24200/sci.2017.4095

Hsieh, M. Y., and Mizuhara, H. (1987). *Silicon nitride having low dielectric constant.* US Patent 4708943

Hsieh, M. Y. (1987). *Low dielectric loss silicon nitride base material.* US Patent 4654315

Kandi, K. K., Thallapalli, N., and Chilakalapalli, S. P. R. (2014). Devolopment of silicon nitride-based ceramic radomes-A review. *Int. J. Appl. Ceram. Technol.* 12, 909–920. doi:10.1111/ijac.12305

Lee, S. W., Chae, H. B., Park, D. S., Choa, Y. H., Niihara, K., and Hockey, B. J. (2000). Thermal conductivity of unidirectionally oriented Si_3N_4w/Si_3N_4 composites. *J. Mater. Sci.* 35 (18), 4487–4493. doi:10.1023/A:1004807516791

Hou, Y. B., Yang, X. J., Li, B., Lia, D., Gaoa, S., and Wua, Z. (2019). Preparation and interface modification of Si_3N_{4f}/SiO_2 composites. *J. Mater. Sci. Technol.* 35 (12), 2767–2771. doi:10.1016/j.jmst.2019.05.069.

Li, Z. Z., Zou, Z. Y., Qin, Y., Qi, M., Ren, J., and Peng, Z. (2020). The effect of fibre content on properties of ceramifiable composites. *Plast. Rubber Compos.* 49, 230–236. doi:10.1080/14658011.2020.1731258

Medding, J. A. (1996). Nondestructive evaluation of zirconium phosphate bonded silicon nitride radomes. Master's thesis. Blacksburg (VA): Virginia Polytechnic Institute and State University

Qi, G., Zhang, C., Hu, H., Cao, F., Wang, S., and Jiang, Y. (2005a). Crystallization behavior of three-dimensional silica fiber reinforced silicon nitride composite. *J. Cryst. Growth.* 284 (1-2), 293–296. doi:10.1016/j.jcrysgro.2005.06.039.

Qi, G. J., Zhang, C. R., Hu, H. F., Cao, S. F., Wang, Q., and Cao, Y. B. (2005b). Preparation of three-dimensional silica fiber reinforced silicon nitride composites using perhydropolysilazane as precursor. *Mater. Lett.* 59 (26), 3256–3258. doi:10.1016/j.matlet.2005.04.057.

Qi, G., Zhang, C., Hu, H., Cao, F., Wang, S. S., and Jiang, Y. (2005c). Three-dimensional silica fiber reinforced silicon nitride-based composites fabricated via different polysilazanes. *Adv. Eng. Mater.* 7 (11), 1043–1046. doi:10.1002/adem.200500104.

Wan, W., Feng, Y. B., Yang, J., Bu, W., and Qiu, T. (2016). Microstructure, mechanical and high-temperature dielectric properties of zirconia-reinforced fused silica ceramics. *Ceram. Int.* 42 (5), 6436–6443. doi:10.1016/j.ceramint.2016.01.063.

Xu, H. H. K., Ostertag, C. P., Braun, L. M., and Lloyd, I. K. (1994). Effects of fiber volume fraction on mechanical properties of SiC-fiber/Si_3N_4-matrix composites. *J. Am. Ceram. Soc.* 77 (7), 1897–1900. doi:10.1111/j.1151-2916.1994.tb07068.x.

Xu, J., Luo, F., and Zhou, W. C. (2020). Dielectric properties of porous reaction-bonded silicon nitride with different additives[J]. *J. Electron. Mater.* 49 (3), 1611–1617. doi:10.1007/s11664-019-07462-6.

Yang, X. J., Li, B., Li, D., Shao, C., and Zhang, C. (2019). High-temperature properties and interface evolution of silicon nitride fiber reinforced silica matrix wave-transparent composite materials. *J. Eur. Ceram. Soc.* 39, 240–248. doi:10.1016/j.jeurceramsoc.2018.09.007.

Zhou, J., Cheng, L., Ye, F., Zhang, L., Liu, Y., Cui, X., et al. (2019a). Effects of heat treatment on mechanical and dielectric properties of 3D Si3N4f/BN/Si3N4 composite by CVI. *J. Eur. Ceram. Soc.* 40 (15), 5305–5315. doi:10.1016/j.jeurceramsoc.2020.06.018

Zhou, J., Ye, F., Cheng, L., li, M., Yue, W., and Wang, Y. (2019b). Microstructure and mechanical properties of Si3N4f/Si3N4 composites with different coatings. *Ceram. Int.* 45 (10), 13308–13314. doi:10.1016/j.ceramint.2019.04.020.

Zou, B., Huang, C., and Chena, M. (2009). Study on the mechanical properties, microstructure and oxidation resistance of Si3N4/Si3N4W/Ti(C7N3) nanocomposites ceramic tool materials. *Int. J. Refract. Metals Hard Mater.* 27 (1), 52–60. doi:10.1016/j.ijrmhm.2008.03.003.

Conflict of Interest: The authors declare that the research was conducted in the absence of any commercial or financial relationships that could be construed as a potential conflict of interest.